Journal of Sound and Vibration (2000) **237**(4), 641–666
doi:10.1006/jsvi.2000.3070, available online at http://www.idealibrary.com on IDEAL®

NON-LINEAR DYNAMICS AND STABILITY OF CIRCULAR CYLINDRICAL SHELLS CONTAINING FLOWING FLUID. PART IV: LARGE-AMPLITUDE VIBRATIONS WITH FLOW

M Amabili†

Dipartimento di Ingegneria Industriale, Università di Parma, Parco Area delle Scienze 181/*A*, *Parma I*-43100, *Italy. E-mail: marco@me.unipr.it*

F. Pellicano

Dipartimento di Scienze dell'Ingegneria, Università di Modena e Reggio Emilia, Via Campi 213/*B*, *Modena I*-41100, *Italy*

AND

M. P. Païdoussis

Department of Mechanical Engineering, McGill University, 817 *Sherbrooke Street W.*, *Montreal, Québec, Canada H3A* 2*K*6

(*Received* 13 *September* 1999, *and in final form* 20 *March* 2000)

The response of a shell conveying fluid to harmonic excitation, in the spectral neighbourhood of one of the lowest natural frequencies, is investigated for different flow velocities. The theoretical model has already been presented in Part I of the present study. Non-linearities due to moderately large-amplitude shell motion are considered by using Donnell's non-linear shallow-shell theory. Linear potential flow theory is applied to describe the fluid-structure interaction by using the model proposed by Païdoussis and Denise. For different amplitudes and frequencies of the excitation and for different flow velocities, the following are investigated numerically: (1) periodic response of the system; (2) unsteady and stochastic motion; (3) loss of stability by jumps to bifurcated branches. The effect of the flow velocity on the non-linear periodic response of the system has also been investigated. Poincaré maps and bifurcation diagrams are used to study the unsteady and stochastic dynamics of the system. Amplitude modulated motions, multi-periodic solutions, chaotic responses, cascades of bifurcations as the route to chaos and the so-called "blue sky catastrophe" phenomenon have all been observed for different values of the system parameters; the latter two have been predicted here probably for the first time for the dynamics of circular cylindrical shells.

1. INTRODUCTION

Shells containing flowing fluids are widely used in engineering applications, in which they are subject to manifold excitations of different kinds, including flow excitations. Usually, these shells are made as thin as possible for weight and cost economy; therefore, their response to such excitations is of great interest.

†Author to whom correspondence should be addressed.

0022-460X/00/440641 + 26 $35.00/0

In almost all past studies, linear shell theory has been used, which is accurate only for vibration amplitudes significantly smaller than the shell thickness. In particular, Païdoussis and Denise [1] considered both clamped and cantilevered shells subjected to axial flow and utilized a travelling wave-type solution, nevertheless satisfying the pertinent boundary conditions, along with a separation of variables method to solve the boundary value problem for the linear fluid–structure interaction. Weaver and Unny [2], on the other hand, investigated the stability of simply supported shells by means of the Fourier transform method to solve the fluid–structure interaction. Païdoussis *et al.* [3] extended this method to coaxial cylindrical shells. Horáček and Zolotarev [4] investigated the effect of different boundary conditions at the shell ends. In the papers [1–4], not only shell stability but also the linear dependence of the natural frequencies of the system on the flow velocity are investigated. These results are also obtained in Part I [5] of the present study.

Other than reference [5], the only other study related to large-amplitude vibrations of shells with flow is due to Selmane and Lakis [6]. They consider the non-linear free vibrations of open and closed circular cylindrical shells with fluid flow by using a hybrid finite element method. The formulation is based on the non-linear Sanders–Koiter shell theory, so that structural non-linearities are taken into account. Results show only the effect of vibration amplitude on vibration frequencies. Only one set of results is given for free vibrations of an open circular cylindrical shell with flowing fluid, showing the non-linearity to be either hardening or softening, depending on the circumferential wavenumber n. No results are presented by Selmane and Lakis [6] for closed circular cylindrical shells with flowing fluid, and the response of a shell to harmonic excitation is not investigated, nor are companion mode participation and the effect of structural damping.

In the present study, the response of a shell conveying fluid to harmonic excitation, in the spectral neighbourhood of one of the lowest natural frequencies, is investigated for different flow velocities. The theoretical model has already been presented in Part I [5] of the present study, where stability in the absence of extraneous, forced excitation is investigated. In particular, non-linearities due to moderately large-amplitude shell motion are considered by using Donnell's non-linear shallow-shell theory, taking into account the effect of viscous structural damping. Linear potential flow theory is applied to describe the fluid–structure interaction by using the model proposed by Païdoussis and Denise [1], as presented in reference [5]. The system is discretized by Galerkin's method, and is investigated by using a model involving seven degrees of freedom (d.o.f.), allowing for travelling wave response of the shell and axisymmetric shell contraction.

Since considerable time has elapsed since the appearance of Parts I and II of this study [5, 7], it is perhaps useful to the reader to summarize the principal findings of the research in Parts I–III [5, 7, 8]. Specifically, in terms of the response to forced excitation, it has been found that axisymmetric modes in the modal expansion for the solution of the problem are extremely important: thus, while taking into account the fundamental axisymmetric mode may yield a hardening behaviour, taking more modes in that series into account dramatically changes the behaviour to softening [7]. In terms of the response of the system, it was found that companion modes are very important in the overall response of the system [5]. Specifically, with the aid of the Païdoussis and Denise fluid-dynamical model, it was found that loss of stability by divergence is very strongly subcritical. Furthermore, it was found that the deflected shape of the buckled shell rotates helicoidally about the axis with increasing flow velocity.‡ Significantly, this solution emerges only provided that companion

‡This is a good place to clarify the highly condensed statement made in this regard in reference [5]. The solution branch "3" concerned (see Figure 8 in reference [5]) is unstable in the sense that, when perturbed by a small increment in velocity, it is unstable. However, for each steady value of the flow velocity, the solution is stable.

modes are taken into account. Finally, for at least the shell investigated, all solutions were found to be static [5], i.e., fixed points in phase space, which suggests that the post-divergence coupled-mode flutter obtained by linear theory and confirmed experimentally may correspond to dynamic divergence rather than flutter. Nevertheless, new calculations for the thinner shell, presented in this paper, show that periodic solutions may be possible in some cases for large flow velocities, but they are *unstable*.

2. RESULTS AND DISCUSSION

Numerical results are carried out for the simply supported ($N_x = 0$) circular cylindrical shell with flowing water *and* external excitation already investigated in Part I–III [5, 7, 8] of the present study, having the following characteristics: $L/R = 2$, $h/R = 0{\cdot}01$, $E = 206 \times 10^9$ Pa, $\rho = 7850$ kg/m^3, $\rho_F = 1000$ kg/m^3 and $v = 0{\cdot}3$. Here L is the length of the shell, R its radius and h its wall thickness, E is the Young's modulus, ρ the shell density, and v the Poisson ratio, ρ_F is the fluid density. The mode considered is $n = 5$, $m = 1$, with a damping ratio $\zeta_{1,n} = 0{\cdot}01$, a linear radian frequency for zero flow velocity $\omega_{1,n} = 2\pi \times 106{\cdot}69$ rad/s and a generally variable amplitude of the non-dimensional external modal excitation $\tilde{f} = f_n/\{h\omega_{1,n}^2 m_1 [2/(\pi L)]$, where f_n is the amplitude of the modal excitation defined in reference [5]. The fluid–structure interaction model of Païdoussis and Denise [1, 5] is used. A non-dimensional fluid velocity V is introduced for convenience, defined as in reference [2] by $V = U/\{(\pi^2/L)[D/(\rho h)]^{1/2}\}$, where U is the dimensional flow velocity, and $D = Eh^3/[12(1 - v^2)]$ is the shell flexural rigidity. It is to be noted that the linear radian frequency varies with the flow velocity V, as already investigated (see Figure 2 in Part I of the present study [5]), and is here denoted by ω_V, i.e., ω_V is a function of V.

2.1. PERIODIC RESPONSE

The first part of the analysis is performed by means of the AUTO software [9] for continuation of the solution and bifurcation of non-linear ordinary differential equations, which has previously been used in Part I [5] to study stability and bifurcation of the equilibrium. It was observed that the undisturbed equilibrium position of the system undergoes a strongly subcritical bifurcation at $V = 3{\cdot}33$, such that a stable bifurcated position exists as of $V = 1{\cdot}31$. Therefore, for flow velocity $1{\cdot}31 < V < 3{\cdot}33$ the undisturbed equilibrium position is linearly stable, but other equilibrium positions coexist. This bifurcation is associated with the (5, 1) mode, i.e., a mode with $n = 5$ circumferential waves and $m = 1$ longitudinal half-wave.

Initially, an external harmonic excitation $\tilde{f} = 0{\cdot}03$ with frequency close to the natural frequency of the mode (5, 1) is considered; this corresponds to the problem studied in Parts II and III [7, 8] of the present study for quiescent fluid ($V = 0$). In Figure 1, the amplitude of oscillation of the Lagrangian co-ordinate $A_{1,n}$ is shown for several values of the fluid velocity, in the case of no companion mode participation, i.e., $B_{1,n} = 0$ (see Parts I and II). The dynamical behaviour shows a softening-type non-linearity for the entire flow velocity range explored. It is interesting to note that the maximum amplitude of oscillation varies with the axial flow velocity V and reaches a minimum around $V = 1{\cdot}3$, that is just before the appearance of the bifurcated equilibrium position ($V = 1{\cdot}31$). Thus, increasing the flow velocity from $V = 0$ to $1{\cdot}3$, the vibration amplitude decreases. After this value, the amplitude increases a great deal with the flow velocity. Therefore, it seems that the effect of

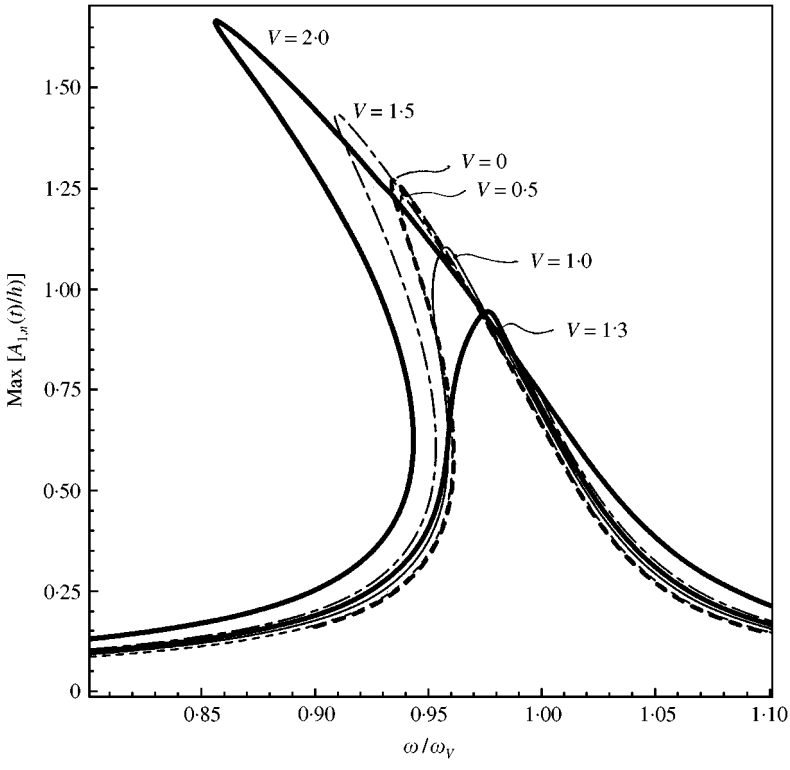

Figure 1. Frequency–response curves for the driven mode without companion mode participation at different flow velocities V; $\tilde{f} = 0{\cdot}03$.

the flow is to reduce the amplitude, the non-linearity and the frequency of the system response up to the velocity corresponding to the instability threshold under disturbance; after this velocity, the frequency of the response is still reduced, but amplitude and non-linearity of the response increase.

In Figure 2, the case of $V = 1$ and $\tilde{f} = 0{\cdot}03$ is analyzed in detail, i.e., the presence of the companion mode is taken into account. The single-mode response, i.e., in the absence of companion mode participation, is typical of softening-type non-linearities. Following branch 1, stability is lost at $\omega/\omega_V = 0{\cdot}9593$ in a folding; then, the system regains stability at $\omega/\omega_V = 0{\cdot}9525$ due to the presence of a second folding. At $\omega/\omega_V = 0{\cdot}9579$ the single-mode response bifurcates and loses stability. After that, in the range $\omega/\omega_V \in (0{\cdot}9579, 1{\cdot}005)$, the companion mode $B_{1,n}$ is excited (see Figure 2(b)). In a narrow region $\omega/\omega_V \in (0{\cdot}96, 0{\cdot}9734)$ both companion mode and single-mode orbits are unstable, which means that the actual orbit is not periodic. Typically, in this region an amplitude modulation due to beating phenomena is present. The main differences with respect to the case for $V = 0$ are: (1) the tip of the response of the driven mode $A_{1,n}$ is rounded and presents an enlarged stable portion, and (2) the companion mode $B_{1,n}$ reaches larger amplitude.

When the flow velocity V is increased to 1·3, corresponding to the last point of safe stability under disturbance [5], the vibration amplitude reaches its minimum; moreover, the amplitude–frequency relationship, shown in Figure 3, assumes a different shape as compared to those obtained for different flow velocities and the same excitation amplitude. In fact, no folding is anymore present on branch 1, and branch 2 is always stable in the region of its existence. The response still presents a slightly softening-type behaviour.

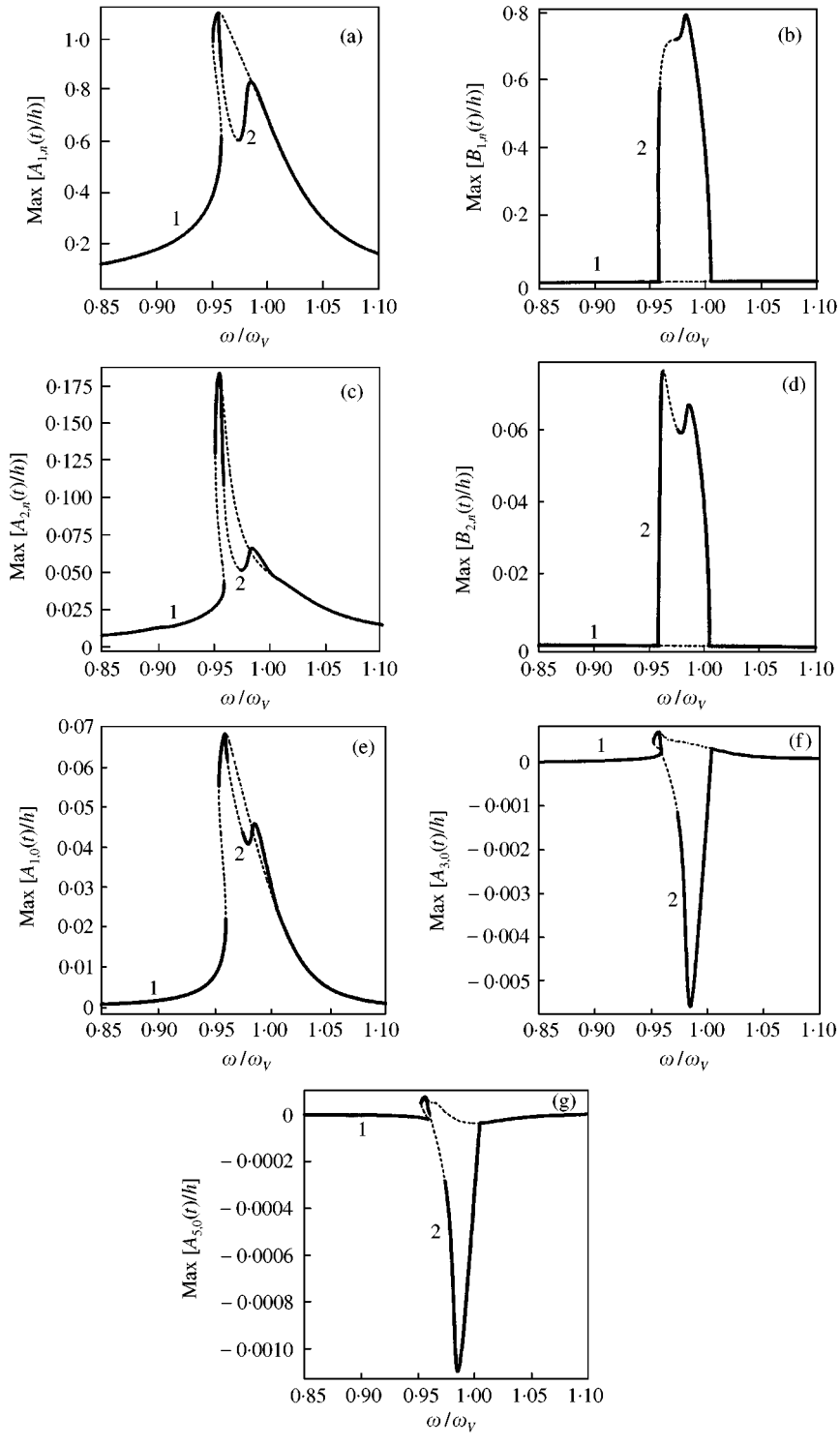

Figure 2. Frequency–response curve with companion mode participation for $V = 1$ and $\tilde{f} = 0{\cdot}03$. (a) Maximum of $A_{1,n}(t)/h$; (b) maximum of $B_{1,n}(t)/h$; (c) maximum of $A_{2,n}(t)/h$; (d) maximum of $B_{2,n}(t)/h$; (e) maximum of $A_{1,0}(t)/h$; (f) maximum of $A_{3,0}(t)/h$; (g) maximum of $A_{5,0}(t)/h$: ——, stable solutions; – – –, unstable solutions.

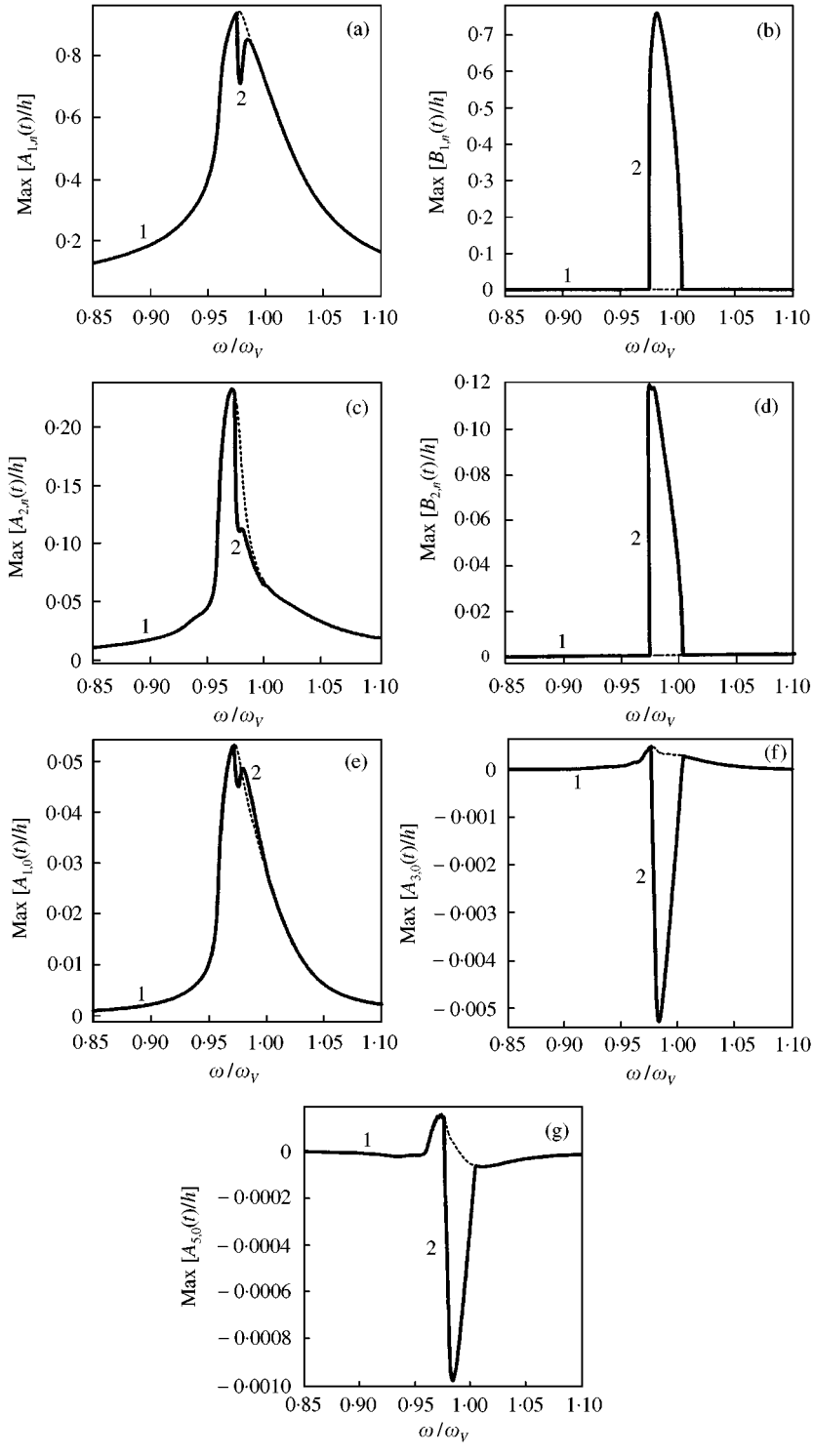

Figure 3. Frequency–response curves with companion mode participation for $V = 1{\cdot}3$ and $\tilde{f} = 0{\cdot}03$: ——, stable solutions; – – –, unstable solutions.

In Figure 4, the case of $V = 2$ and a 10-fold augmented excitation amplitude $\tilde{f} = 0{\cdot}3$ is studied. The single-mode response loses stability at $\omega/\omega_V = 0{\cdot}8679$ in branch 1, through a folding. Then, it regains stability at $\omega/\omega_V = 0{\cdot}775$ via a second folding. At $\omega/\omega_V = 0{\cdot}7955$ the orbit loses stability for the second time and remains unstable up to the bifurcation point, $\omega/\omega_V = 1{\cdot}0045$, where a solution branch including the companion mode arises. Companion mode participation is present in the region $\omega/\omega_V \in (0{\cdot}1426,\ 1{\cdot}0045)$. This branch of the periodic orbit has a pitchfork bifurcation at $\omega/\omega_V = 0{\cdot}6886$; from this point, a third bifurcated branch arise, which ends at $\omega/\omega_V = 0{\cdot}6818$, where it merges with the second branch. It should be noted that the second branch loses stability at $\omega/\omega_V = 0{\cdot}6470$, through

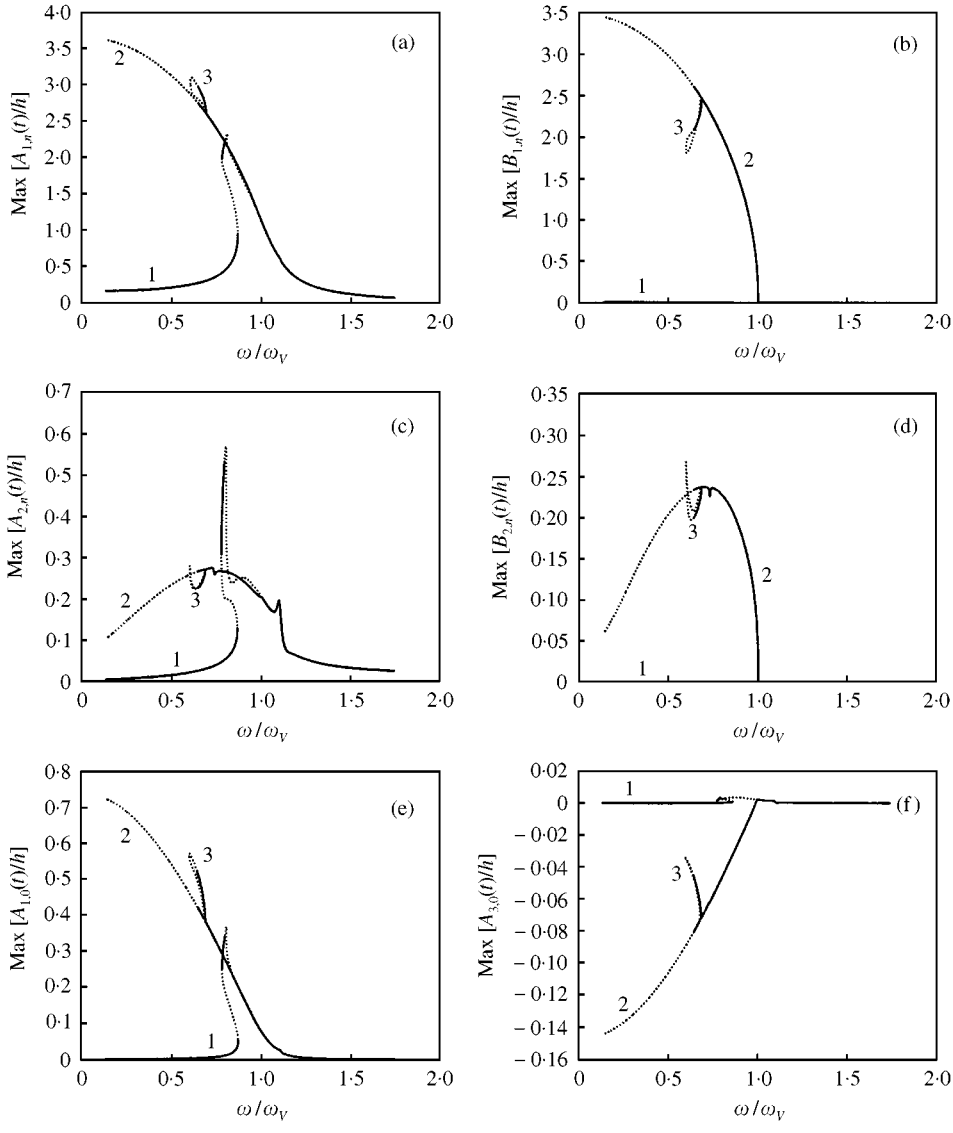

Figure 4. Frequency–response curve with companion mode participation for $V = 2$ and $\tilde{f} = 0.3$. (a) Maximum of $A_{1,n}(t)/h$; (b) maximum of $B_{1,n}(t)/h$; (c) maximum of $A_{2,n}(t)/h$; (d) maximum of $B_{2,n}(t)/h$; (e) maximum of $A_{1,0}(t)/h$; (f) maximum of $A_{3,0}(t)/h$; (g) maximum of $A_{5,0}(t)/h$: (h) particular of (a); (i) particular of (b): ——, stable solutions; – – –, unstalbe solutions.

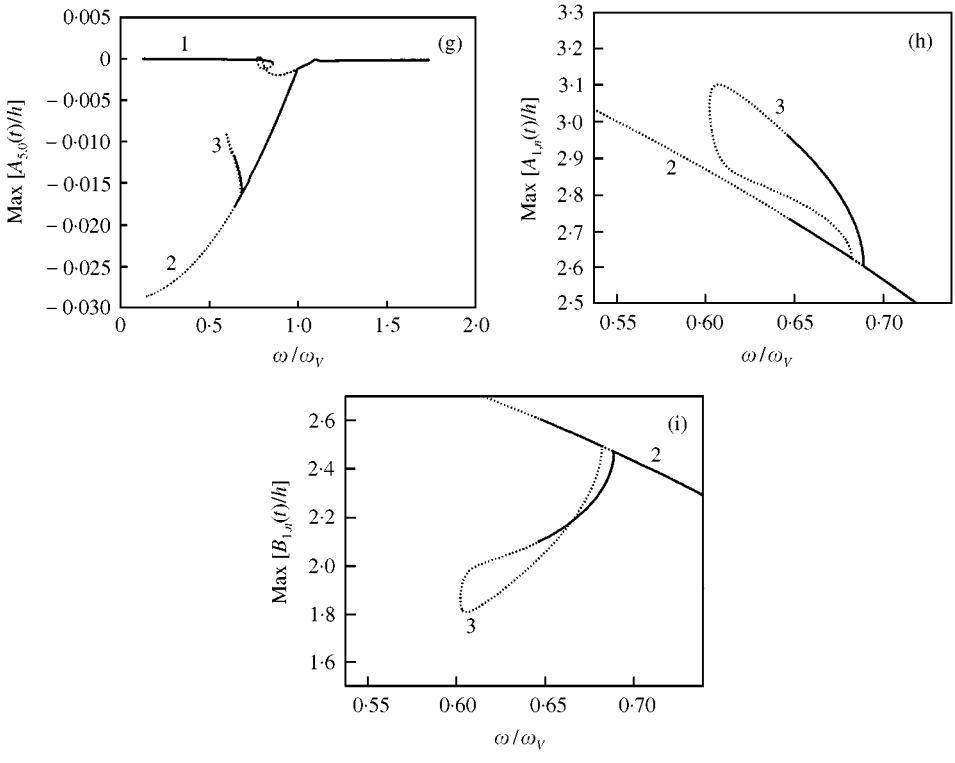

Figure 4. Continued.

a torus bifurcation, and that the third branch loses stability at $\omega/\omega_V = 0{\cdot}6458$, via a period-doubling bifurcation. It is interesting to note that the periodic orbit including companion mode participation displays a different shape when compared with the classical cases of cylindrical shells without flow and with cases involving smaller flow velocity. In fact, in this case, the second branch ends at $\omega/\omega_V = 0{\cdot}1426$, where the interaction with the bifurcated equilibrium position destroys the periodic orbit and does not permit a continuation of the solution.

The dynamics of the system around the bifurcated equilibrium position $A_{1,n} = 0$, $B_{1,n} = 0$, $A_{2,n} = 0$, $B_{2,n} = 6{\cdot}17524$, $A_{1,0} = 1{\cdot}68391$, $A_{3,0} = 1{\cdot}32631$, $A_{5,0} = -0{\cdot}696408$ is analyzed for $V = 2$, $\tilde{f} = 0{\cdot}1$ and the results are shown in Figure 5. The first branch represents almost the whole of the single-mode response because companion mode participation is small. This branch loses stability at $\omega/\omega_V = 2{\cdot}367$ through a folding (see Figure 5(a)). When companion mode participation becomes effective, i.e., when the first branch bifurcates at $\omega/\omega_V = 2{\cdot}245$ and the second branch (branch 2) arises, the system response moves away from the initial equilibrium position. In particular, the second branch ends in the neighbourhood of a second bifurcated equilibrium position where $A_{1,n}$, $B_{1,n}$ and $B_{2,n}$ are close to zero and $A_{2,n}$ is close to $\pm 6{\cdot}17$; around this equilibrium position the periodic orbit regains stability. It is to be noted that the resonance frequency for small vibration amplitudes around the bifurcated position studied is about 2·5 times the linear frequency ω_V for oscillations around the undisturbed position for the same flow velocity. It means that the system presents higher resonance frequencies on the bifurcated branches, i.e., it is stiffer.

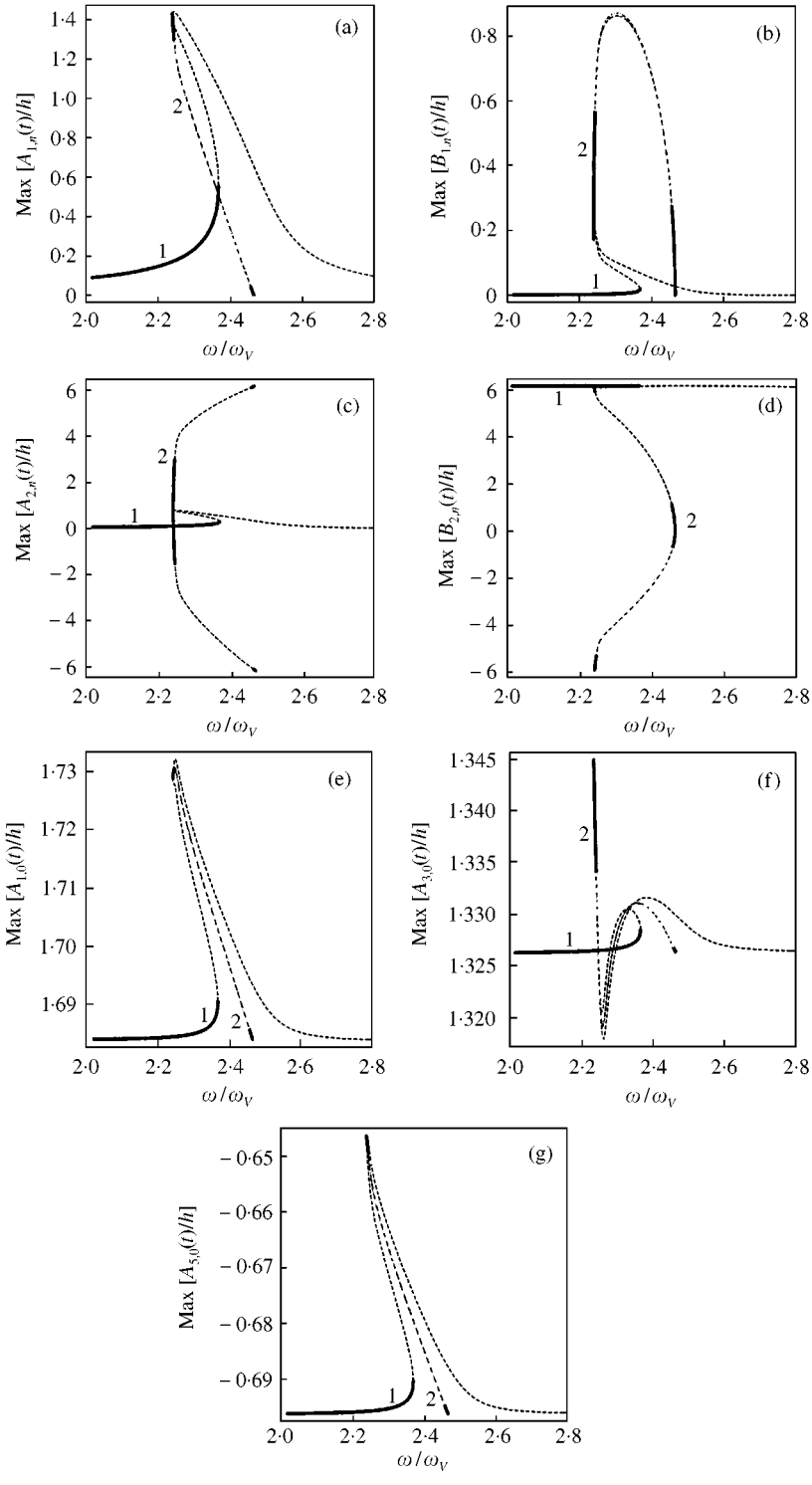

Figure 5. Frequency–response curve with companion mode participation starting from a bifurcated position for $V = 2$ and $\tilde{f} = 0{\cdot}1$. (a) Maximum of $A_{1,n}(t)/h$; (b) maximum of $B_{1,n}(t)/h$; (c) maximum of $A_{2,n}(t)/h$; (d) maximum of $B_{2,n}(t)/h$; (e) maximum of $A_{1,0}(t)/h$; (f) maximum of $A_{3,0}(t)/h$; (g) maximum of $A_{5,0}(t)/h$: ——, stable solutions; – – –, unstable solutions.

2.2. UNSTEADY AND STOCHASTIC MOTION

In this section, direct numerical simulations are performed by using the adaptive step-size fourth–fifth order Runge–Kutta method. The aim is to investigate the dynamic behaviour of the system when periodic solutions lose stability. Different kinds of behaviour have been found: (1) periodic harmonic and subharmonic response: (2) periodic response with amplitude modulation; (3) chaotic motion; (4) jumps from undisturbed positions to bifurcated ones during oscillation.

The first tool used here to investigate parametrically the dynamic behaviour of the system is the Poincaré map and the corresponding bifurcation diagram. In the case of external periodic excitation and in the presence of damping, the Poincaré map coincides with the T-map, which is obtained by sampling the time history at the frequency of the external excitation. Because the dimension of the system is larger than two, Poincaré sections are projected on the planes spanned by each d.o.f. and its velocity, for example $(A_{1,n}, \dot{A}_{1,n})$. When a parameter of the system varies, generally, Poincaré maps change with a certain continuity, in the case of regular motion. Therefore, it is interesting to follow the evolution of the map when a parameter is varied. In order to represent the evolution of the Poincaré map, a projection of a single Lagrangian co-ordinate onto a plane is usually effected; such a sequence of projections is also called a bifurcation diagram of the Poincaré maps.

In Figure 6, such a bifurcation diagram is shown. The excitation frequency is close to the linear frequency (including the flow effect) of mode (5, 1) for $V = 2$, i.e., $\omega/\omega_V = 1{\cdot}07446$, with the companion mode not being active. The variable parameter in this case is the excitation amplitude $\tilde{f}$. For small amplitude of the excitation, a sequence of single points is observed, i.e., a single point is obtained for any fixed $\tilde{f}$. This point corresponds to periodic response with the same frequency as the external excitation. When $\tilde{f} = 0{\cdot}1444$ the periodic orbit loses stability, and an amplitude-modulated motion takes place. At $\tilde{f} = 0{\cdot}2519$ the amplitude modulation orbit loses stability and a $5T$ orbit arises, where a $5T$ orbit means that the system response is periodic with a period 5 times larger than the excitation period T. The $5T$ orbit loses stability for $\tilde{f} = 0{\cdot}2612$, where a succession of chaotic and multiple-T periodic orbit regions starts. This region ends at $\tilde{f} = 0{\cdot}2940$, and a stable $9T$ orbit occurs, up to $\tilde{f} = 0{\cdot}3125$. Increasing the force, another chaotic region arises, and this chaotic orbit collapses at $\tilde{f} = 0{\cdot}3359$; at this value of $\tilde{f}$, the energy furnished to the system is large enough to allow a jump, which leads the system to orbit around the bifurcated position with

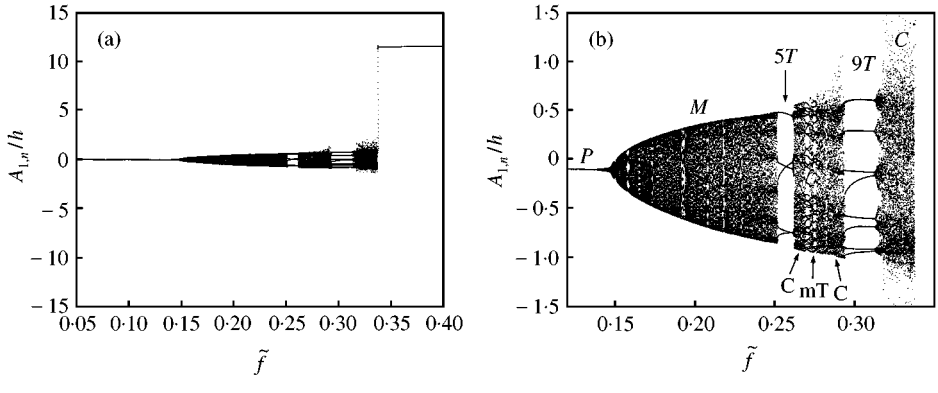

Figure 6. Bifurcation diagram without companion mode participation for $\omega/\omega_V = 1{\cdot}07446$ and $V = 2$. (a) $A_{1,n}(t)/h$; (b) enlarged view of (a). P, simple periodic motion; M, modulated amplitude; 5T, 9T and mT, periodic motion of multiple period; C, chaotic response.

a simple orbit of period T. In Figure 6(b), "P" indicates simple periodic motion, "M" amplitude-modulated response, "5T", "9T" and "mT" are used for periodic obit of multiple period and "C" is the label for chaotic response.

It is interesting to analyze the effect of companion mode participation on the dynamics of the system. To this end, the previous analysis was repeated by perturbing slightly the companion mode. In Figure 7, the bifurcation diagrams for all seven d.o.f.s are presented; in particular, Figure 7(a, h) shows the equivalent of Figure 6(a, b). It is seen that the periodic orbit loses stability at $\tilde{f} = 0{\cdot}1444$, while the companion mode is not excited up to $\tilde{f} = 0{\cdot}2057$; then an amplitude-modulated orbit emerges, and it collapses into a chaotic orbit at $\tilde{f} = 0{\cdot}27$. A jump occurs at $\tilde{f} = 0{\cdot}3364$, where the chaotic orbit around the undisturbed fixed point collapses into periodic orbit around the bifurcated equilibrium position. In Figure 7(h), "P" indicates simple periodic motion, "M" amplitude-modulated response, and "C" chaotic motion.

The previous results show that the force level $\tilde{f} = 0{\cdot}3$ is interesting for the study of the system dynamics and therefore a further investigation is performed for this value of $\tilde{f}$, this time varying the excitation frequency. In Figure 8, the bifurcation diagram is shown in the frequency range $\omega/\omega_V \in (0{\cdot}53,\ 1{\cdot}13)$. The companion mode is perturbed from zero and participates in the response. Two quite interesting frequency intervals are found: $\omega/\omega_V \in (0{\cdot}7631,\ 0{\cdot}7717)$ and $\omega/\omega_V \in (1{\cdot}0432,\ 1{\cdot}123)$. When the excitation frequency decreases and reaches the value 0·7717, the periodic orbit bifurcates (see Figure 8(h, i)) and the system moves on a new periodic orbit which loses stability at $\omega/\omega_V = 0{\cdot}7640$. Then a $3T$ periodic orbit arises; this loses stability and a chaotic orbit is present in the narrow region $\omega/\omega_V \in (0{\cdot}7631,\ 0{\cdot}7634)$. When the excitation frequency grows to $\omega/\omega_V = 1{\cdot}0432$, the periodic T orbit loses stability and is replaced by an amplitude-modulated orbit (see Figure 8(j, k)), which is stable up to $\omega/\omega_V = 1{\cdot}0583$. Then, the period $9T$ orbit, already met in the previous results, appears. This orbit suddenly loses stability at $\omega/\omega_V = 1{\cdot}0643$ and this gives rise to a chaotic region. This sudden change of behaviour is often called a "blue sky catastrophe". The companion mode participation is present for $1{\cdot}073 < \omega/\omega_V < 1{\cdot}083$. Then, at $\omega/\omega_V = 1{\cdot}083$, the chaotic orbit is replaced by an amplitude-modulated motion, the nature of which changes at $\omega/\omega_V = 1{\cdot}105$. Finally, an unexpected jump is present at $\omega/\omega_V = 1{\cdot}123$. After this value, the system behaviour becomes a regular periodic motion around the bifurcated position. In Figure 8(h, j), "P" indicates simple periodic motion, "M" amplitude-modulated response, "3T" and "9T" are used for periodic orbit of multiple period, and "C" denotes chaotic response.

The three previous bifurcation diagrams indicate several sets of system parameters for which complex dynamics takes place. These regions should be investigated further. To this end, time histories, power spectra and Poincaré maps will be shown for the most interesting parameter values.

In order to analyze the $9T$ periodic orbit, the system behaviour is investigated for the following parameter values: $\omega/\omega_V = 1{\cdot}07446$, $\tilde{f} = 0{\cdot}3$ and $V = 2$; note that the $9T$ orbit is present when the companion mode is not excited. In Figure 9, time histories, phase portraits, a power spectrum and a Poincaré map are shown. The time histories show an amplitude-modulated motion, which actually corresponds to a closed trajectory in the phase plane. Note that the phase plots are shown for a very long time history, i.e., the integration time is more than 10 times the excitation period. Nevertheless, the phase trajectory does not fill the intervening phase space; this behaviour is typical of periodic or quasiperiodic motions, but not chaotic ones. The power spectrum in Figure 9(e) shows that the frequency peaks are not incommensurable; specifically, the fundamental frequency of the signal is 1/9th of the excitation frequency and the frequency distance δ between the peaks is equal to $\delta = 0{\cdot}2388\omega_{1,n}$. Moreover, the maximum energy of the signal is located in

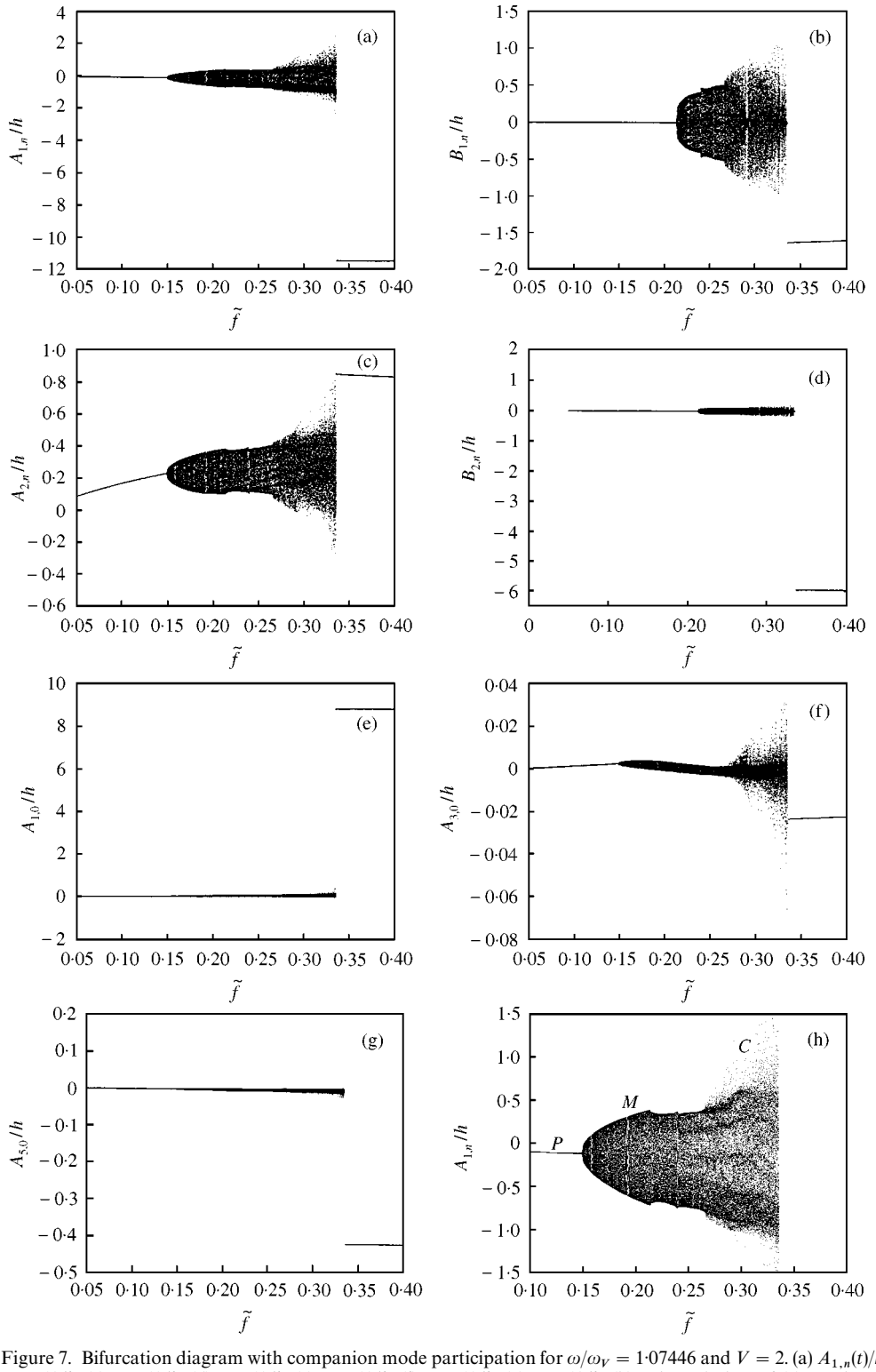

Figure 7. Bifurcation diagram with companion mode participation for $\omega/\omega_V = 1{\cdot}07446$ and $V = 2$. (a) $A_{1,n}(t)/h$; (b) $B_{1,n}(t)/h$; (c) $A_{2,n}(t)/h$; (d) $B_{2,n}(t)/h$; (e) $A_{1,0}(t)/h$; (f) $A_{3,0}(t)/h$; (g) $A_{5,0}(t)/h$; (h) enlarged view of (a): P, simple periodic motion; M, modulated amplitude; C, chaotic response.

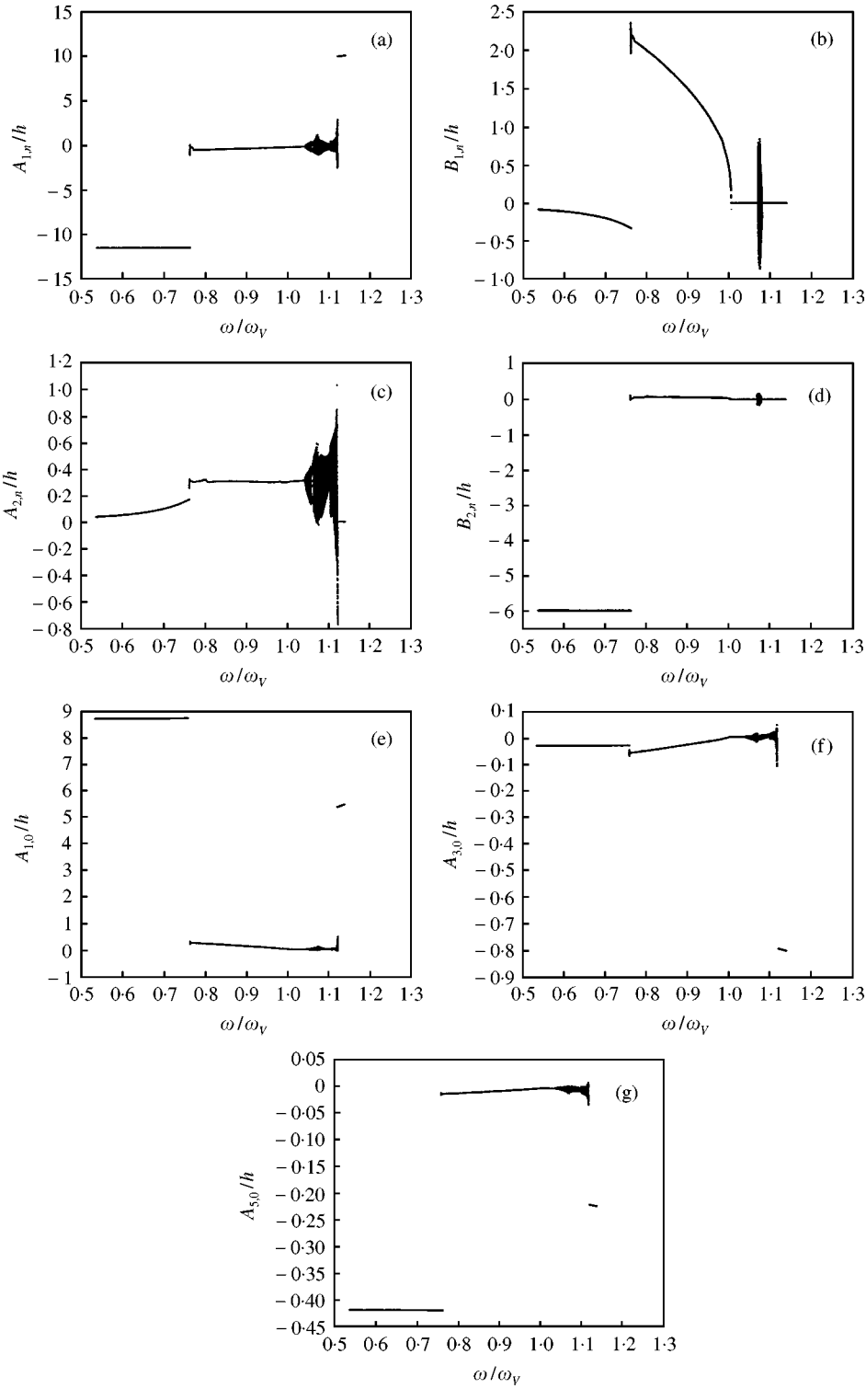

Figure 8. Bifurcation diagram with companion mode participation for $\tilde{f} = 0{\cdot}3$ and $V = 2$. (a) $A_{1,n}(t)/h$; (b) $B_{1,n}(t)/h$; (c) $A_{2,n}(t)/h$; (d) $B_{2,n}(t)/h$; (e) $A_{1,0}(t)/h$; (f) $A_{3,0}(t)/h$; (g) $A_{5,0}(t)/h$; (h) enlarged view of (a) for $0{\cdot}75 < \omega/\omega_V < 0{\cdot}78$; (i) enlarged view of (b) for $0{\cdot}75 < \omega/\omega_V < 0{\cdot}78$; (j) enlarged view of (a) for $1 < \omega/\omega_V < 1{\cdot}15$; (k) enlarged view of (b) for $1 < \omega/\omega_V < 1{\cdot}15$: P, simple periodic motion; M, modulated amplitude; 3T and 9T, periodic motion of multiple period; C, chaotic response.

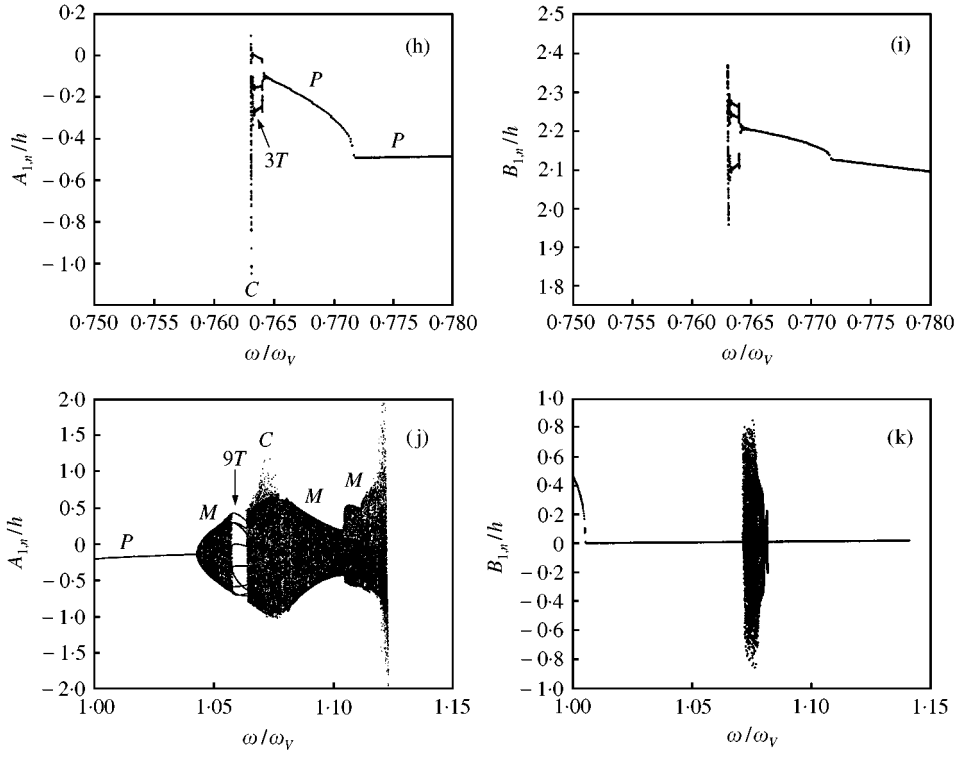

Figure 8. Continued. (see caption on page 653).

correspondence to the excitation frequency. Figure 9(f) shows the Poincaré map projected on the $(A_{1,n}, \dot{A}_{1,n})$ plane, where nine isolated points are present, proving that the motion is not quasiperiodic but a $9T$ periodic orbit.

The previous case is now considered with companion mode participation. In Figure 10, time histories, phase portraits, power spectra and Poincaré maps are shown. The time history given in Figure 10(a) shows an amplitude-modulated motion, which is qualitatively similar to the previous case. Note that the companion mode, Figure 10(b), is excited and gives rise to an irregular motion. The phase plots show that the phase trajectory fills the phase space, which is a typical behaviour of unsteady motions. This situation is more clear in the power spectra of $A_{1,n}$ and $B_{1,n}$, Figure 10(e–f); the spectra are highly polluted, i.e., the signal energy spreads around each peak, over the whole spectrum. The fundamental frequency of the signal is still visible at 1/9th of the excitation frequency in Figure 10(e) and the frequency separation between the peaks is still equal to $\delta = 0{\cdot}2388\omega_{1,n}$; moreover, if Figures 10(e) and 9(e) are superposed, the peaks coincide. This indicates that the chaotic trajectory with companion mode participation is a perturbation of the $9T$ periodic orbit previously shown in Figures 9(a–d) without companion mode participation. Another interesting phenomenon is observed by comparing Figures 10(e) and 10(f); in fact, the peaks in the response of the companion mode $B_{1,n}$ are shifted to lower frequencies by $\delta/2$ with respect to peaks in the response of $A_{1,n}$. Figures 10(g–h) show the Poincaré maps projected on planes spanned by $(A_{1,n}, \dot{A}_{1,n})$ and $(B_{1,n}, \dot{B}_{1,n})$, where a strange attractor is found to be present. It is interesting to note that the presence of the companion mode destroys the periodic orbit and causes the onset of chaotic motion. However, this chaotic

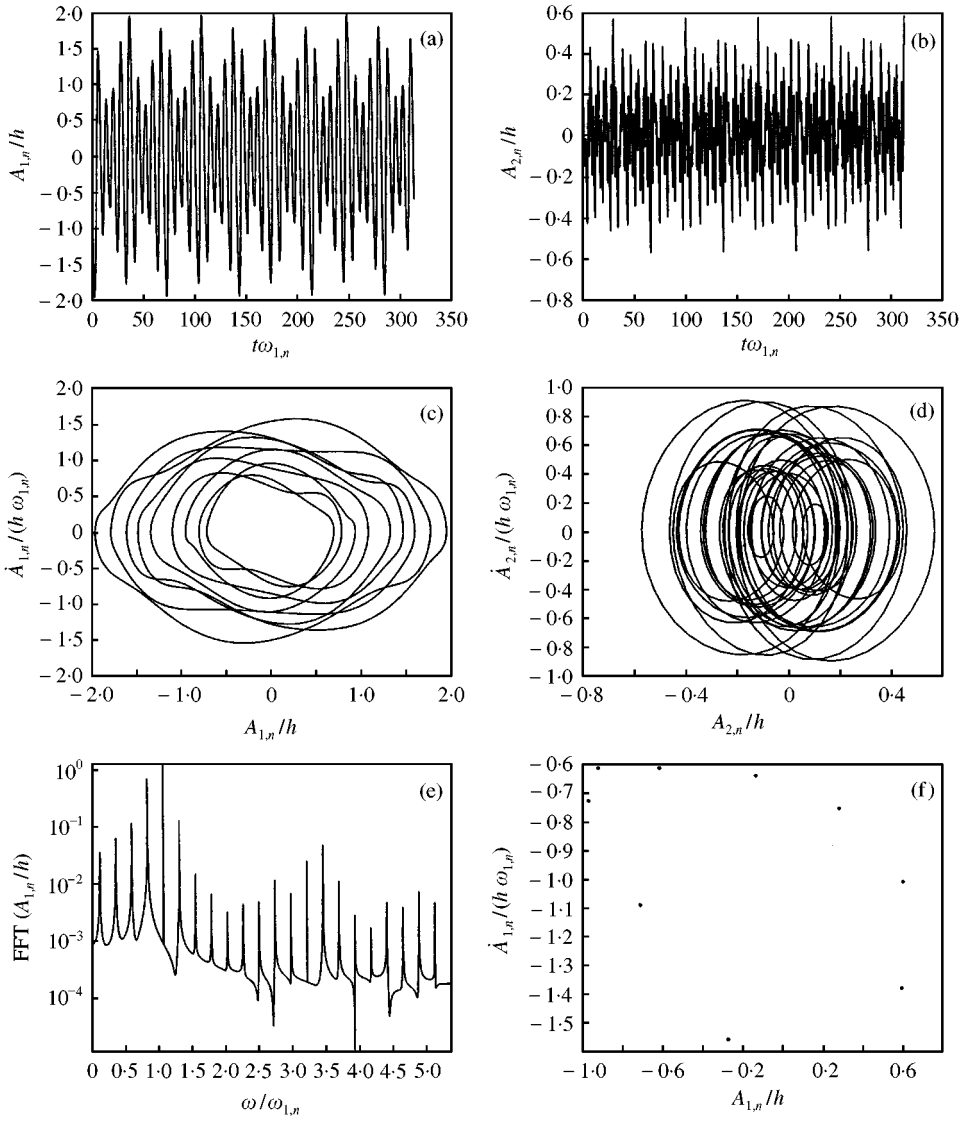

Figure 9. Response of the system without companion mode participation for $\tilde{f} = 0{\cdot}3$, $\omega/\omega_V = 1{\cdot}07446$ and $V = 2$. (a) Time response of the generalized co-ordinate $A_{1,n}(t)/h$; (b) time response $A_{2,n}(t)/h$; (c) phase portrait of $A_{1,n}(t)/h$; (d) phase portrait of $A_{2,n}(t)/h$; (e) power spectrum of $A_{1,n}(t)/h$; (f) Poincaré map in the plane $\{A_{1,n}(t)/h, \dot{A}_{1,n}(t)/(h\omega_V)\}$.

trajectory is a perturbation of the unstable $9T$ periodic orbit, as clarified by the power-spectral analysis.

A second interesting case is obtained for $\tilde{f} = 0{\cdot}3$, $V = 2$ and around the frequency ratio $\omega/\omega_V = 0{\cdot}7635$. Only the Poincaré maps are shown here, for brevity. Figure 11 shows that for $\omega/\omega_V = 0{\cdot}7635$ the system dynamics is governed by a $3T$ periodic orbit with companion mode participation. Figures 12 and 13 are for $\omega/\omega_V = 0{\cdot}7634$ and $0{\cdot}7632$, respectively, and show the chaotic attractors that appear after the collapse of the periodic orbit. The maps are quite complex; in particular, they incorporate several limit cycles and at least two saddle

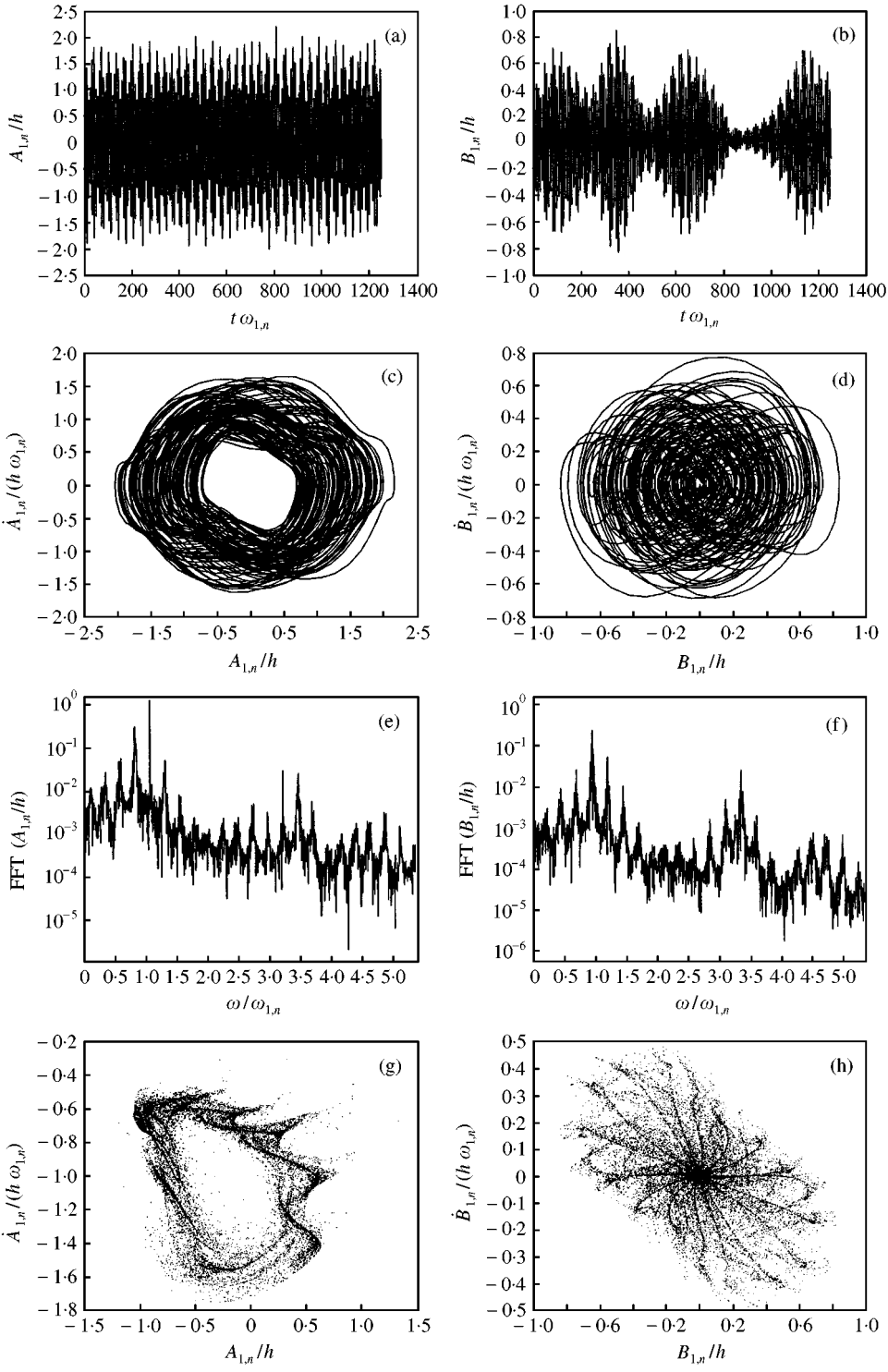

Figure 10. Response of the system with companion mode participation for $\tilde{f} = 0{\cdot}3$, $\omega/\omega_V = 1{\cdot}07446$ and $V = 2$. (a) Time response $A_{1,n}(t)/h$; (b) time response $B_{1,n}(t)/h$; (c) phase portrait of $A_{1,n}(t)/h$; (d) phase portrait of $B_{1,n}(t)/h$; (e) power spectrum of $A_{1,n}(t)/h$; (f) power spectrum of $B_{1,n}(t)/h$; (g) Poincaré map in the plane $\{A_{1,n}(t)/h,\, \dot{A}_{1,n}(t)/(h\omega_V)\}$; (*h*) Poincaré map in the plane $\{B_{1,n}(t)/h,\, \dot{B}_{1,n}(t)/(h\omega_V)\}$.

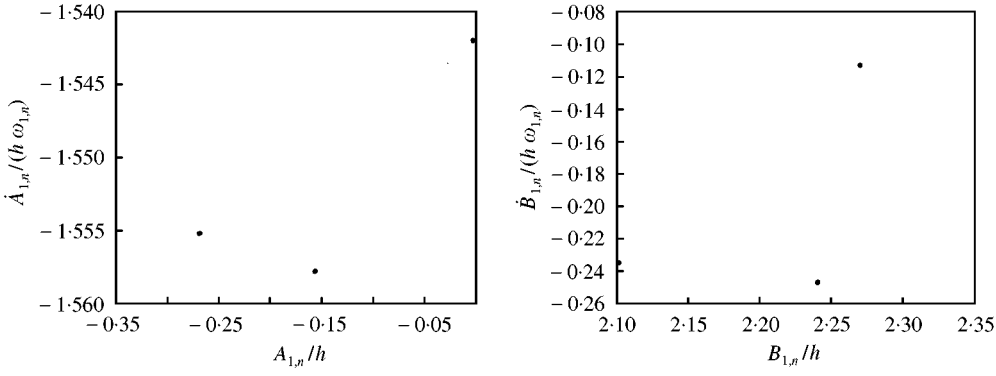

Figure 11. Poincaré maps for $\tilde{f} = 0{\cdot}3$, $\omega/\omega_V = 0{\cdot}7635$ and $V = 2$: (a) $A_{1,n}(t)/h$; (b) $B_{1,n}(t)/h$.

nodes. Note that the analysis of multi-dimensional Poincaré maps is quite complex and is beyond the scope of the present work. Here it is just interesting to observe that the system undergoes quite different types of dynamical behaviour; simple periodic motion, multi-T motions and chaotic dynamic can appear, by changing slightly the system parameters.

Lastly, in Figure 14, the bifurcation diagram versus the axial flow velocity is shown for $\tilde{f} = 0{\cdot}3$ and $\omega/\omega_V = 1{\cdot}07446$. The companion mode becomes active for $0 < V < 1{\cdot}903$ and $1{\cdot}991 < V < 2{\cdot}059$. A periodic motion of period $T = 2\pi/\omega$ is present for $V \in (0, 1{\cdot}818)$ and $V > 2{\cdot}15$. An amplitude- modulated motion takes place in the range $V \in (1{\cdot}818, 1{\cdot}847)$; the limit cycle in the Poincaré map loses stability for $V = 1{\cdot}847$ and is replaced by a chaotic attractor. The chaotic orbit loses the companion mode participation for $V = 1{\cdot}903$. Another chaotic region with active companion mode arises in the range $V \in (1{\cdot}991, 2{\cdot}043)$; it is replaced by a limit cycle attractor at $V = 2{\cdot}043$ which is stable up to $V = 2{\cdot}15$.

2.3. LOSS OF STABILITY BY JUMPS TO BIFURCATED BRANCHES

The last investigation performed is related to the loss of stability by jumps from the undisturbed positions to the bifurcated branches for flow velocity $1{\cdot}31 < V < 3{\cdot}33$ with harmonic excitation. This phenomenon gives a violent buckling (divergence) of the shell that usually causes failure in applications. Direct numerical simulations have been performed by using the adaptive step-size-fourth–fifth order Runge–Kutta method for a few flow velocities, varying the amplitude and the frequency of the excitation $\tilde{f}$. It has been found that, for $V = 2$, an excitation amplitude $\tilde{f} = 0{\cdot}15$ at frequency $\omega/\omega_V = 0{\cdot}8$ is necessary to obtain the jump shown in Figure 15. It is interesting to observe that only the driven mode $A_{1,n}$ is directly excited: however, after a while, the system displays a quite regular helicoidal motion and finally reaches the bifurcated branch. If the amplitude is reduced or the frequency changed, then no jumps are obtained for $\tilde{f} = 0{\cdot}15$.

Similarly, for $V = 2{\cdot}8$, it is necessary to have an excitation amplitude $\tilde{f} = 0{\cdot}048$ at frequency $\omega/\omega_V = 0{\cdot}79$ to obtain the jump (see Figure 16). By reducing the amplitude or changing the frequency for $\tilde{f} = 0{\cdot}048$, again no jumps are obtained. Therefore, when the non-dimensional flow velocity V is increased from 2 to 2·8, the excitation amplitude necessary for the jump is reduced by a factor of three.

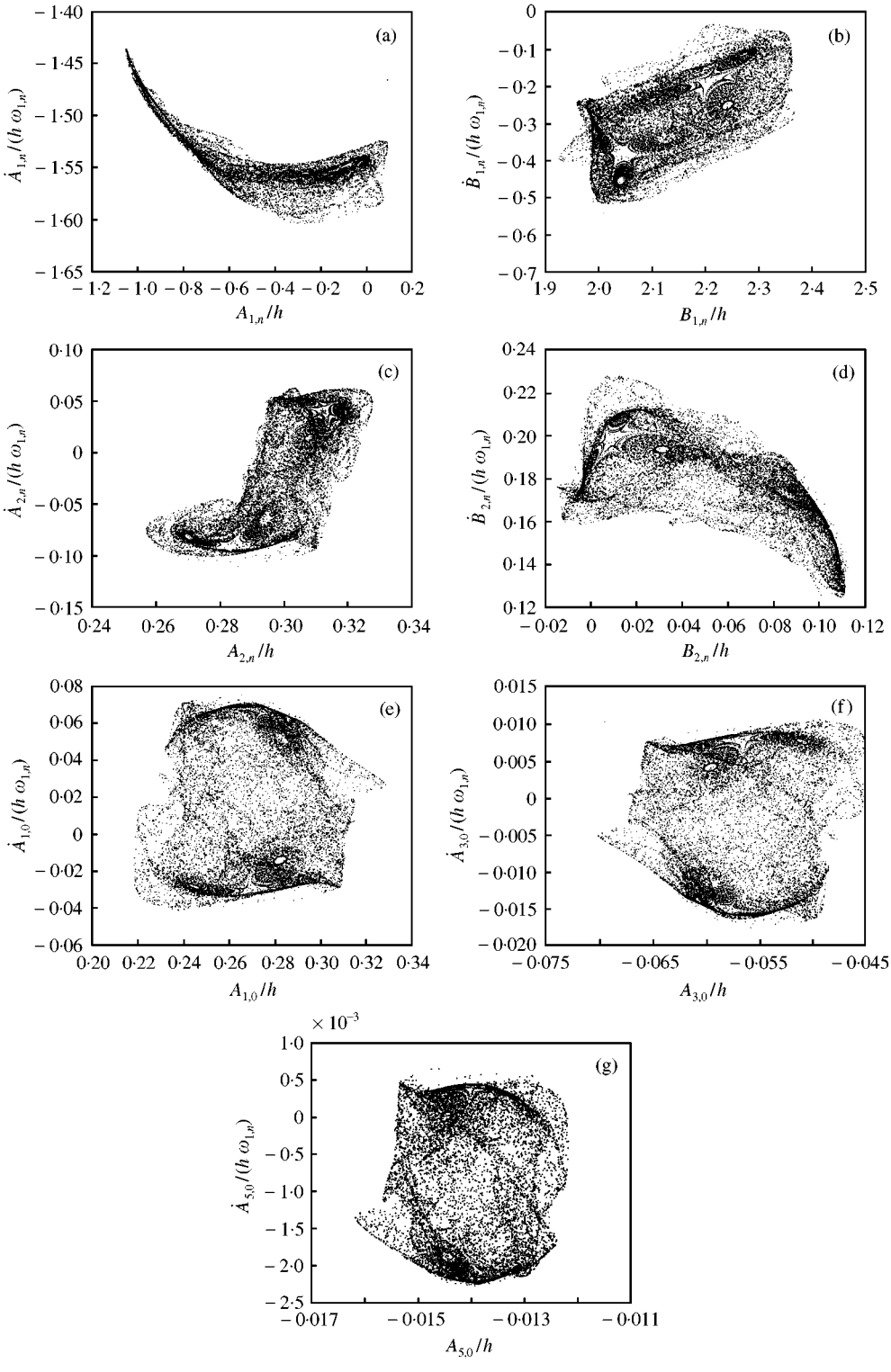

Figure 12. Poincaré maps for $\tilde{f} = 0{\cdot}3$, $\omega/\omega_V = 0{\cdot}7634$ and $V = 2$: (a) $A_{1,n}(t)/h$; (b) $B_{1,n}(t)/h$; (c) $A_{2,n}(t)/h$; (d) $B_{2,n}(t)/h$; (e) $A_{1,0}(t)/h$; (f) $A_{3,0}(t)/h$; (g) $A_{5,0}(t)/h$.

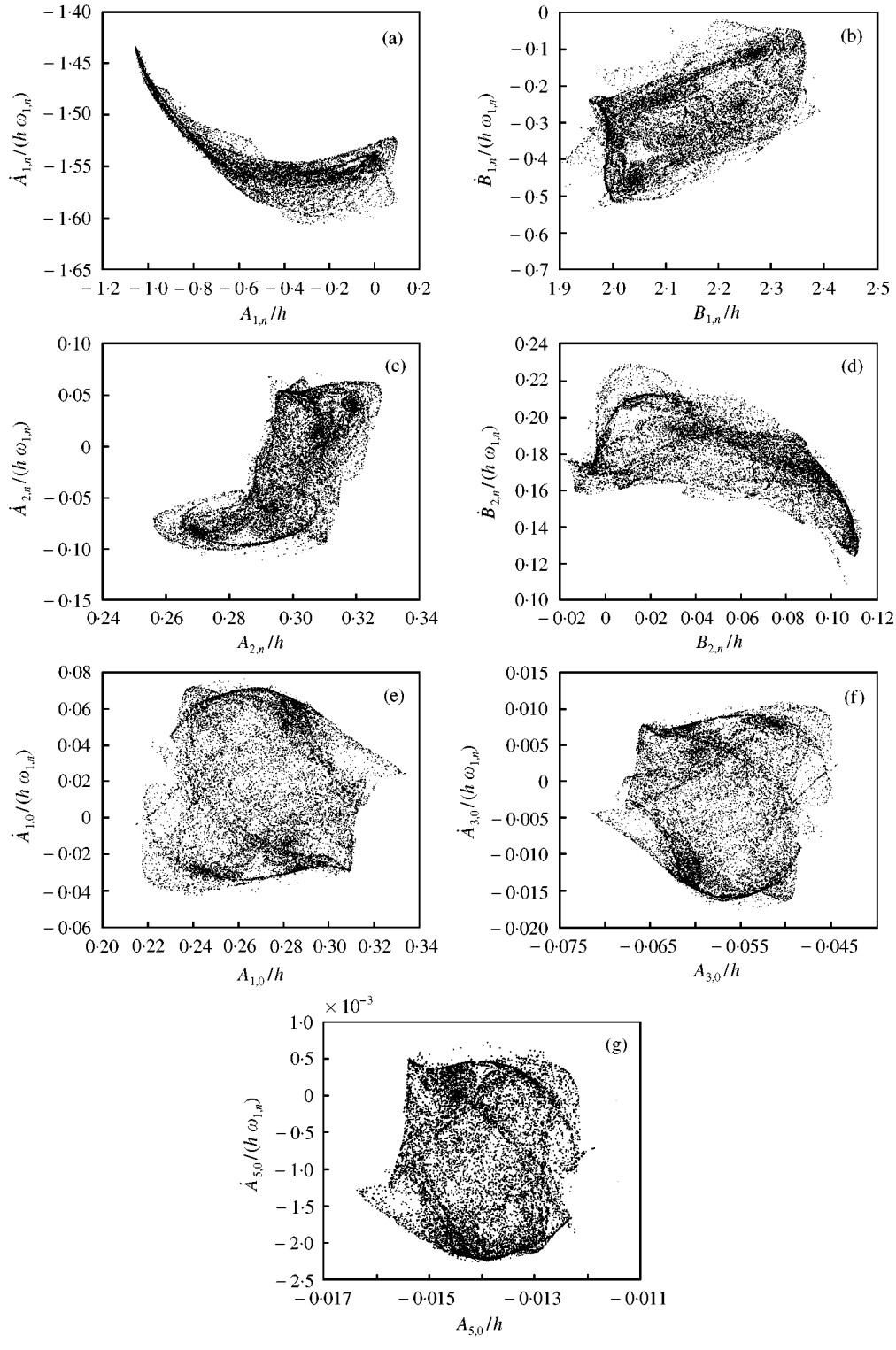

Figure 13. Poincaré maps for $\tilde{f} = 0{\cdot}3$, $\omega/\omega_V = 0{\cdot}7632$ and $V = 2$: (a) $A_{1,n}(t)/h$; (b) $B_{1,n}(t)/h$; (c) $A_{2,n}(t)/h$; (d) $B_{2,n}(t)/h$; (e) $A_{1,0}(t)/h$; (f) $A_{3,0}(t)/h$; (g) $A_{5,0}(t)/h$.

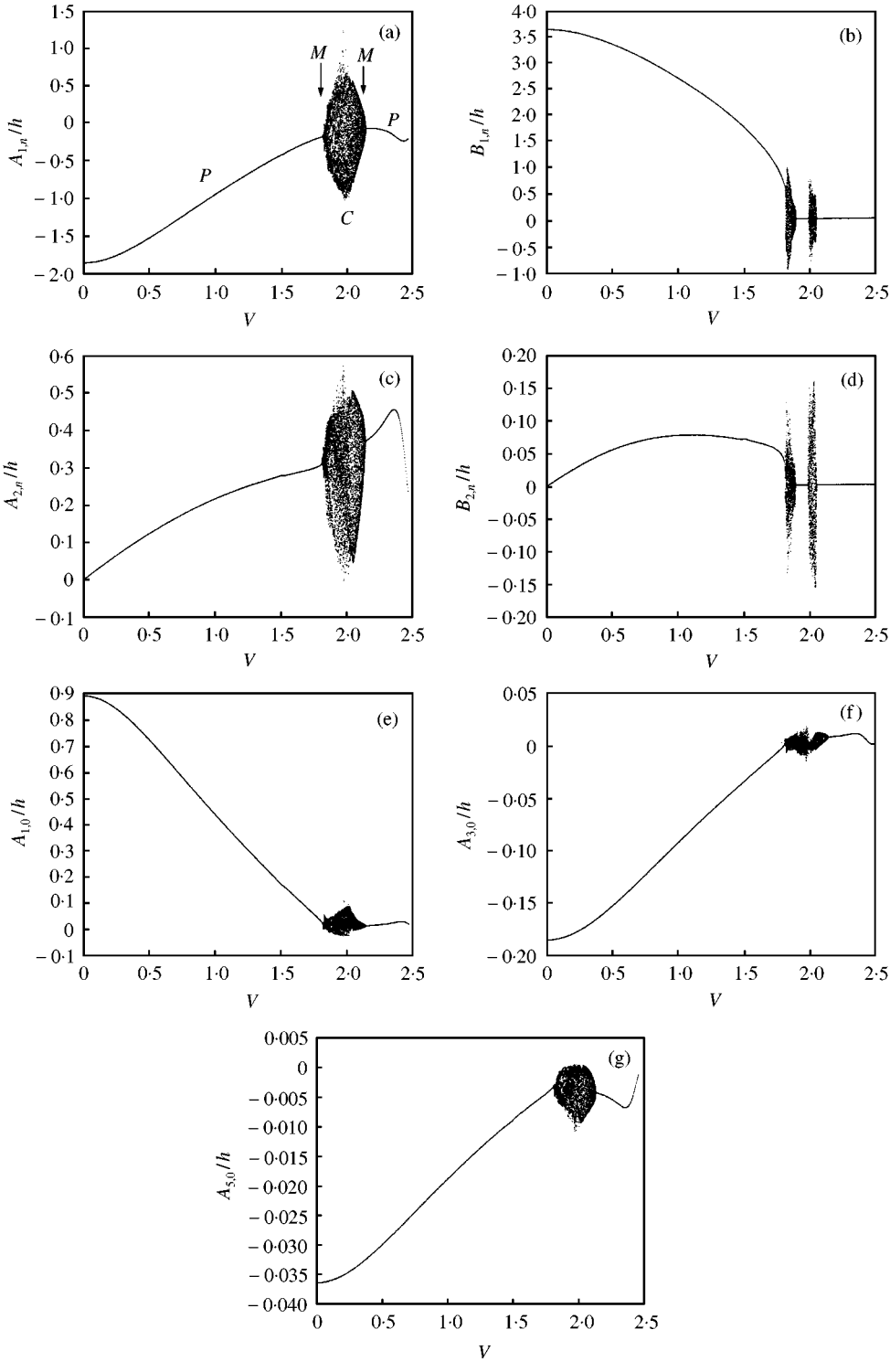

Figure 14. Bifurcation diagram with companion mode participation for $\tilde{f} = 0{\cdot}3$ and $\omega/\omega_V = 1{\cdot}07446$. (a) $A_{1,n}(t)/h$; (b) $B_{1,n}(t)/h$; (c) $A_{2,n}(t)/h$; (d) $B_{2,n}(t)/h$; (e) $A_{1,0}(t)/h$; (f) $A_{3,0}(t)/h$; (g) $A_{5,0}(t)/h$: P, simple periodic motion; M, modulated amplitude; C, chaotic response.

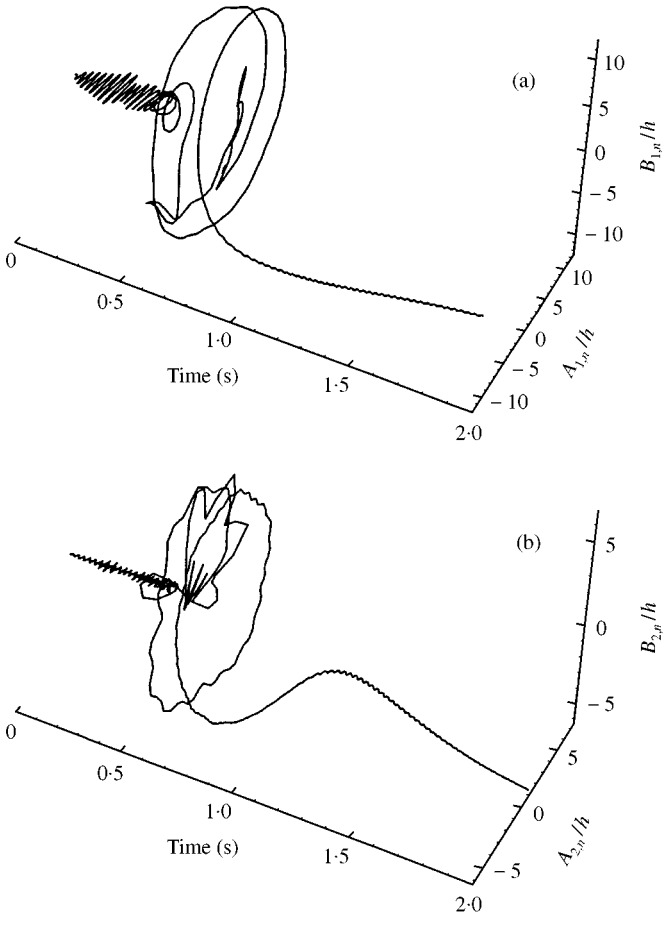

Figure 15. Time response for $\tilde{f} = 0{\cdot}15$, $\omega/\omega_V = 0{\cdot}8$ and $V = 2$: (a) Axial mode $m = 1$; (b) axial mode $m = 2$.

3. ADDITIONAL RESULTS FOR STABILITY OF A THINNER SHELL

In section 2 of the present paper and in Part I of this study [5], a circular cylindrical shell with thickness ratio $h/R = 0{\cdot}01$ is considered. Here the same shell but with a 10-fold reduced thickness ratio, $h/R = 0{\cdot}001$, is considered in order to further investigate the possibility of periodic solutions (post-divergence coupled-mode flutter) for the system without external excitation. Figures 17 and 18 are analogous to Figures 4 and 8, respectively, in reference [5]. In particular, Figure 17 is for a solution with in-phase asymmetric modes ($B_{1,n} = B_{2,n} = 0$), and Figure 18 with asymmetric modes orthogonal in θ ($B_{1,n} = A_{2,n} = 0$), as already discussed [5]. So far as divergence is concerned, the curves are qualitatively similar to those obtained in Part I [5] for a thicker shell, with the main difference being that now the linear divergence is predicted for flow velocity $V = 7{\cdot}77$[§] while the minimum flow for the onset of divergence (given a sufficient disturbance, actually quite large, in this case) is $V = 1{\cdot}41$; it means that divergence can be possible for a flow velocity 5·5 times less than that computed

[§] It may appear strange that the crictical V here is *larger* than that for the thicker shell, but this is because we have used Weaver and Unny's non-dimensionalization scheme; the dimensional flow velocity is in fact smaller for the thinner shell.

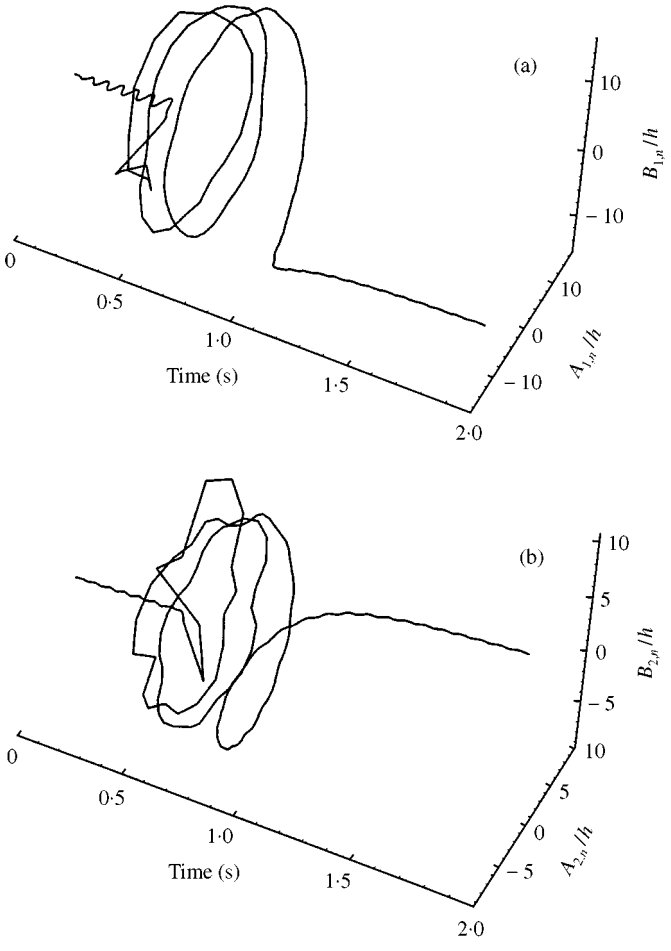

Figure 16. Time response for $\tilde{f} = 0{\cdot}048$, $\omega/\omega_V = 0{\cdot}79$ and $V = 2{\cdot}8$: (a) Axial mode $m = 1$; (b) axial mode $m = 2$.

by linear theory! Actually, the shell displacement associated with divergence in this case is so large that the shell theory used cannot give accurate results.

It is interesting to observe that for $V \geqslant 12{\cdot}6$ periodic solutions are possible, see Figures 17(c–e). In particular, in Figures 17(c–d) the branches corresponding to the maximum value of the generalized co-ordinate are indicated by the superscript $'$ (e.g., $4'$) and those corresponding to the minimum value of the generalized co-ordinate are indicated by the superscript $''$ (e.g., $4''$). However all the solutions obtained by using the AUTO software [8] are *unstable*. It means that, for large flow velocity, periodic solutions are in principle possible, also without external excitation, but they do not appear to be simple periodic solutions; they could be quasiperiodic, amplitude-modulated or even chaotic solutions. Actually, direct integration of the equations of motion performed by using an adaptive step-size Runge–Kutta integration scheme in the range $20 \geqslant V \geqslant 12{\cdot}6$ shows that, for different initial conditions, the system is always subject to coupled-mode divergence with asymmetric modes orthogonal in θ, i.e., the stable attractive solution is branch "3" of Figure 18 which is a static solution. The response of this thinner shell to harmonic excitation is expected to be even more complicated than that in the previous section for large V.

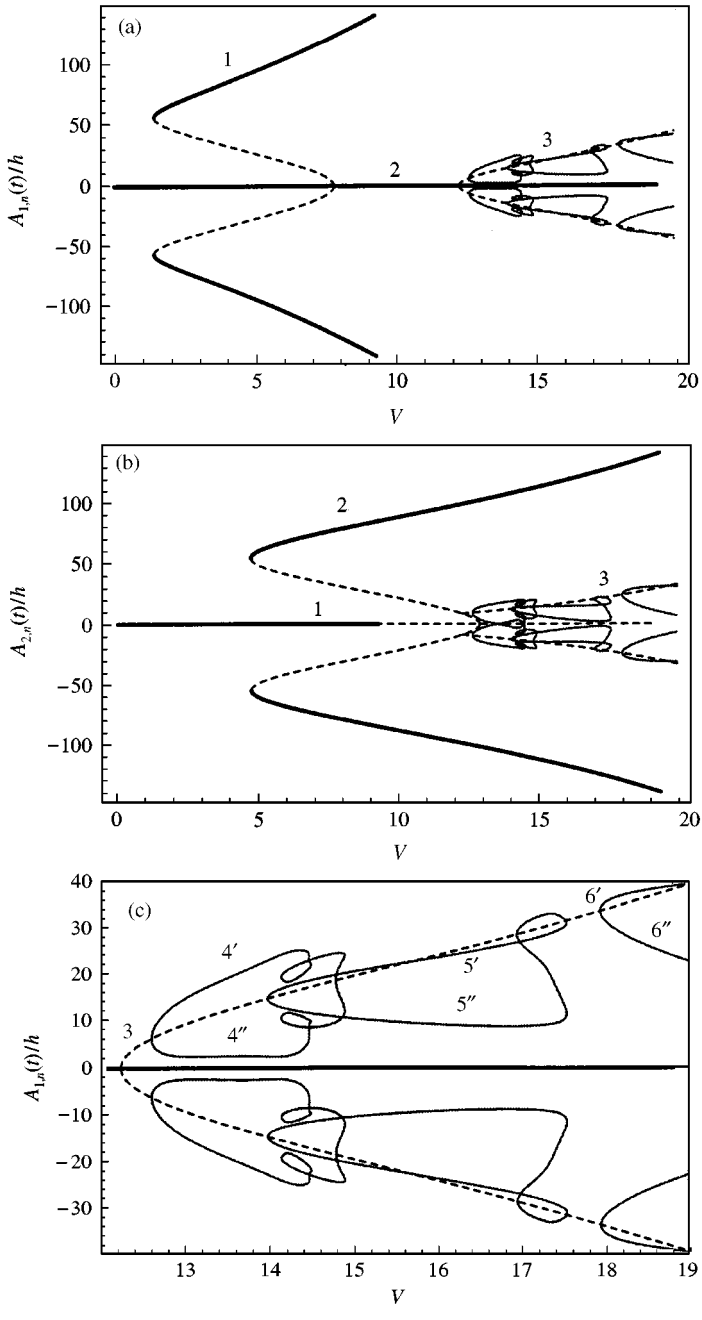

Figure 17. Non-oscillatory and periodic oscillatory solutions without external excitation versus the non-dimensional flow velocity V; in-phase modes: ———, stable non-oscillatory branches; – – –, unstable non-oscillatory branches; ——, unstable oscillatory solutions: (a) amplitude of the first longitudinal mode $A_{1,n}/h$; (b) amplitude of the second longitudinal mode $A_{2,n}/h$; (c) enlarged view of (a); (d) enlarged view of (b); (e) frequency of oscillatory solutions versus V.

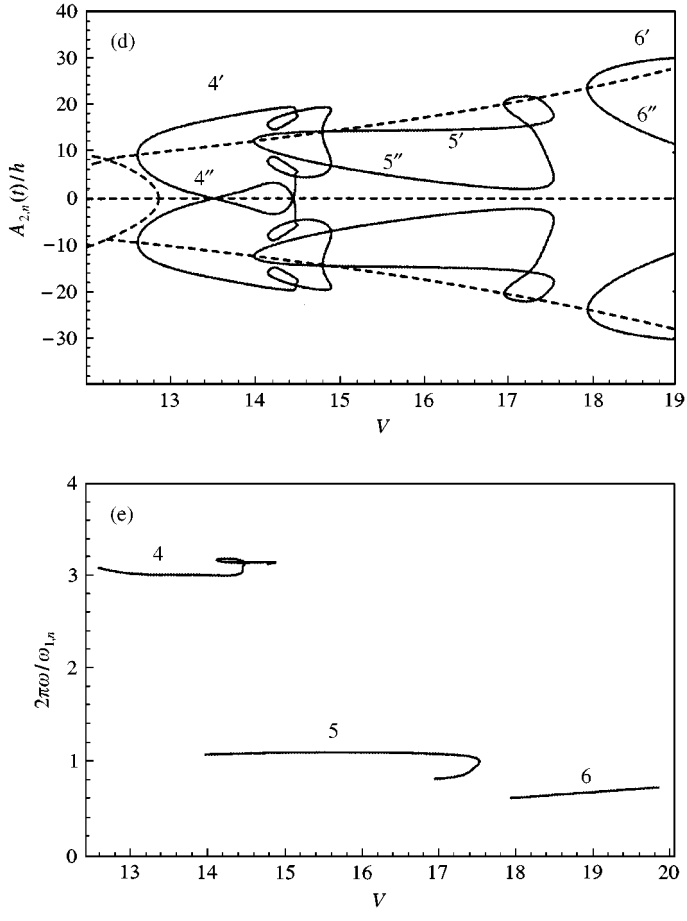

Figure 17. Continued.

4. DISCUSSION AND CONCLUSIONS

As the discussion of the individual figures in section 2 has *perforce* been quite detailed, and perhaps tedious, here some of the overall features of the results are discussed, hopefully giving a broad appreciation of what has been obtained.

The first observation is that, as the flow velocity is increased from zero, (1) the degree of softening of the response diminishes, up to the point ($V = 1{\cdot}3$) where the subcritical pitchfork bifurcation indicates that divergence is possible, given enough perturbation, and (2) the degree of softening increases thereafter (see Figure 1). Non-linear effects begin to dominate the response for this higher-V range, since linear stiffness begins to tend towards vanishing, which occurs at $V = 3{\cdot}33$, the linear divergence threshold.

The second observation is that, for a fixed V, the modal content of the frequency–response curves, see Figures 2–5, changes dramatically with ω. Some components of the response become unstable, while others remain stable for the same specific values of ω. The unstable components indicate that, in the parts of the frequency–response curve concerned, the response is not periodic, signalling that it could be quasiperiodic or chaotic. With increasing excitation amplitude up to a certain value, the frequency–response curve becomes much more complex, as can be appreciated by comparing Figures 2 and 4.

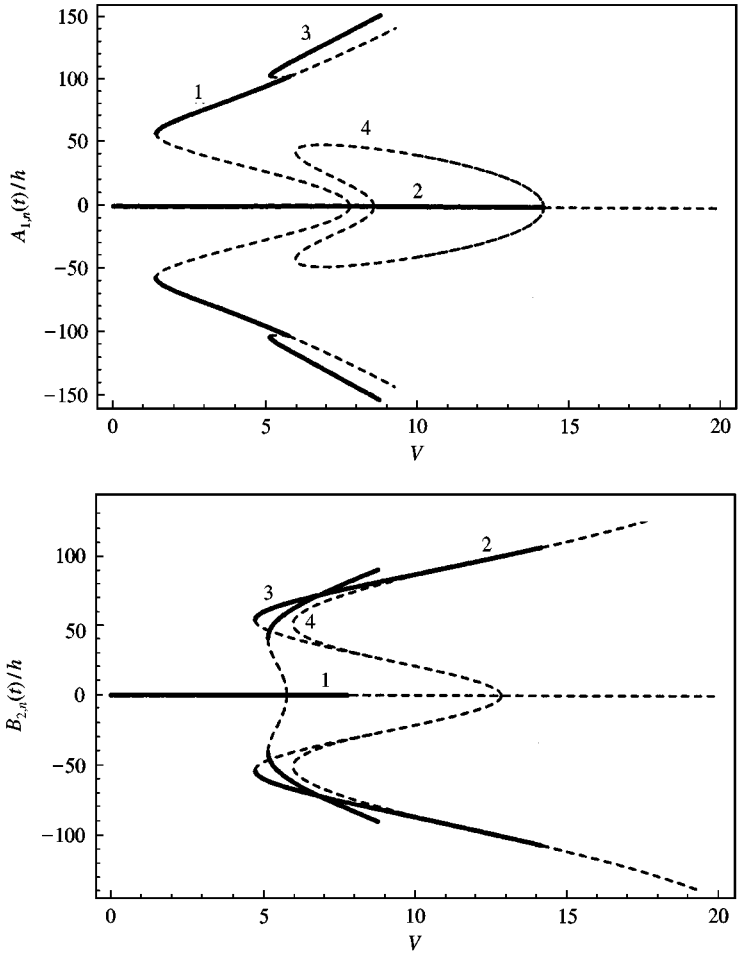

Figure 18. Non-oscillatory solutions without external excitation versus the non-dimensional flow velocity V; orthogonal modes: ———, stable non-oscillatory branches; – – –, unstable non-oscillatory branches; (a) amplitude of the first longitudinal mode $A_{1,n}/h$; (b) amplitude of the second longitudinal mode $B_{2,n}/h$.

The existence of (1) quasiperiodic, amplitude-modulated response, (2) period-3 ($3T$), period-5 ($5T$) and period-9 ($9T$) responses, and (3) chaos for sufficiently large (but not *too* large) $\tilde{f}$ is confirmed by the bifurcation diagrams of Figures 6 and 7. Significantly, with companion mode participation, the multi-T periodic windows vanish and are absorbed by the quasiperiodic surrounding regions of the bifurcation diagram. These observations are supported and confirmed by time-traces, phase-plane diagrams, power spectra and Poincaré maps. With companion mode participation the very interesting phenomenon of the so-called "blue sky catastrophe" is observed for $\tilde{f}$ large enough (Figure 8), whereby a very sudden, "explosive" or "catastrophic" change in the response occurs.

Comparing qualitatively the response without and with companion-mode participation, the latter being the "true" response, the following observation is made. The presence of the companion mode introduces a degree of fuzziness in the response, as may be seen by comparing Figure 9(a,c,e,f) to Figure 10(a,c,e,g). This makes also clear the usefulness of the companion-mode-free calculations: they help us to understand the more complicated-looking results with companion mode participation.

The final comment relates to the subcritical pitchfork bifurcation obtained in Part I for the shell with fluid flow but no mechanical forced excitation, extending over $1{\cdot}31 < V < 3{\cdot}33$. It is shown in Figures 15 and 16 that, given enough forced excitation, the system will jump for the stable (trivial) equilibrium, over the unstable branch, and onto the higher, stable solution (buckled form). Furthermore, the route to this stable state is shown to follow a helicoidally evolving deformation.

This concludes the tetralogy (Parts I–IV) on flow-induced and mechanically forced deformation/motion of a shell by means of the simple theory developed in Part I. What has been found is quite important; however, what remains to be done is equally significant and extensive. The results obtained must be reconfirmed by calculations with several other sets of system parameters and by experiments.

ACKNOWLEDGMENTS

This work was partially supported by a grant of the Italian Space Agency (ASI). The last author also expresses his gratitude to NESRC of Canada and FCAR of Québec for their support. The support of Programme québécois de bourses d'excellence of the Ministère de l' Éducation du Québec is acknowledged for the visit of the first author to McGill University in the summer of 1999.

REFERENCES

1. M. P. Païdoussis and J.-P Denise 1972 *Journal of Sound and Vibration* **20**, 9–26. Flutter of thin cylindrical shells conveying fluid.
2. D. S. Weaver and T. E. Unny 1973 *Journal of Applied Mechanics* **40**, 48–52. On the dynamic stability of fluid-conveying pipes.
3. M. P. Païdoussis, S. P. Chan and A. K. Misra 1984 *Journal of Sound and Vibration* **97**, 201–235. Dynamics and stability of coaxial cylindrical shells containing flowing fluid.
4. J. Horáček and I. Zolotarev 1984 *Soviet Applied Mechanics* **20**, 756–765. Influence of fixing edges of a cylindrical shell with conveying fluid on its dynamic characteristics.
5. M. Amabili, F. Pellicano and M. P. Païdoussis 1999 *Journal of Sound and Vibration* **225**, 655–699. Non-linear dynamics and stability of circular cylindrical shells containing flowing fluid. Part I: stability.
6. A. Selmane and A. A. Lakis 1997 *Journal of Sound and Vibration* **202**, 67–93. Non-linear dynamic analysis of orthotropic open cylindrical shells subjected to a flowing fluid.
7. M. Amabili, F. Pellicano and M. P. Païdoussis 1999 *Journal of Sound and Vibration* **228**, 1103–1124. Non-linear dynamics and stability of circular cylindrical shells containing folowing fluid, Part II: large-amplitude vibrations without flow.
8. M. Amabili, F. Pellicano and M. P. Païdoussis 2000 *Journal of Sound and Vibration* **237**, 617–640. Non-linear dynamics and stability of circular cylindrical shells containing flowing fluid. Part III: truncation effect without flow and experiments.
9. E. J. Doedel, A. R. Champneys, T. F. Fairgrieve, Y. A. Kuznetsov, B. Sandstede and X. Wang 1998 *AUTO* 97: *Continuation and Bifurcation Software for Ordinary Differential Equations* (*with HomCont*). Concordia University, Montreal, Canada.